Bipolar electrode focusing: tuning the electric field gradient†

Robbyn K. Anand,[a] Eoin Sheridan,[a] Dzmitry Hlushkou,[b] Ulrich Tallarek*[b] and Richard M. Crooks*[a]

Received 28th August 2010, Accepted 28th October 2010
DOI: 10.1039/c0lc00351d

Bipolar electrode (BPE) focusing is a developing technique for enrichment and separation of charged analytes in a microfluidic channel. The technique employs a bipolar electrode that initiates faradaic processes that subsequently lead to formation of an ion depletion zone. The electric field gradient resulting from this depletion zone focuses ions on the basis of their individual electrophoretic mobilities. The nature of the gradient is of primary importance to the performance of the technique. Here, we report dynamic measurements of the electric field gradient showing that it is stable over time and that its axial position in the microchannel is directly correlated to the location of an enriched tracer band. The position of the gradient can be tuned with pressure-driven flow. We also show that a steeper electric field gradient decreases the breadth of the enriched tracer band and therefore enhances the enrichment process. The slope of the gradient can be tuned by altering the buffer concentration: higher concentrations result in a steeper gradient. Coating the channel with the neutral block co-polymer Pluronic also results in enhanced enrichment.

Introduction

In this paper, we report time-resolved measurements of the electric field gradient responsible for bipolar electrode (BPE) focusing in microchannels,[1] and correlate the location and slope of the gradient to the position and breadth of an enriched band of a fluorescent tracer. The results provide important new information about the fundamental parameters that affect the focusing process. These include the buffer concentration, flow rate, applied field strength, and the effect of a neutral, polymeric coating on the microchannel walls. These observations are significant, because they provide a basis for understanding and optimizing concentration enrichment driven by BPE focusing. The key findings of this study are threefold. First, when left unperturbed, the electric field gradient remains stable over long periods of time (hundreds of seconds). This is consistent with previously published numerical simulations for this system.[2] Second, the location and slope of the electric field gradient, which control the position and breadth of the enriched band, can be tuned by adjusting the flow rate and buffer concentration, respectively. Finally, addition of a neutral polymeric coating to the microchannel walls enhances enrichment by reducing Taylor dispersion and preventing bubble formation at the BPE even at high average field strength (V_m). This results in a steeper slope of the electric field gradient and therefore a higher degree of enrichment.

We have previously reported that a BPE can be used to alter the local electric field within a microchannel in a predictable way, and that the resulting field gradient can be used to concentrate and separate charged analytes.[2–5] Specifically, when a voltage is applied to driving electrodes situated in reservoirs at the ends of a microchannel filled with an electrolyte solution, but lacking a BPE, the applied voltage (E_{tot}) is dropped approximately linearly over the length of the channel. The resulting electric field is illustrated by the dashed line in Fig. 1d. However, when a BPE is present in the channel (Fig. 1a and b), faradaic reactions may take place at its ends (Fig. 1c). This provides an alternative path for current flow, and hence distorts the distribution of electrolyte ions within the channel. This in turn causes the simple linear voltage drop to adopt a more complex shape and gives rise to a gradient in the electric field. To illustrate this point, the solid line in Fig. 1d shows a typical field profile (confirmed by experimental measurements and simulations)[2] in the region adjacent to the BPE cathode and depicts the resulting enrichment of a fluorescent anionic tracer. As discussed later, enrichment is driven by the interplay between bulk flow and electrophoretic migration.

Analyte preconcentrators are a key component of lab-on-a-chip devices (LoCs).[6] One of the many advantages of LoCs is that they are capable of rapidly processing minute sample volumes (nanolitres) using networks of microchannels.[6] Many LoC applications, such as medical diagnostics, require analysis of analytes present at low concentrations. However, detection limit often suffers because the small cross-sectional area interrogated by the detector, coupled with low analyte concentration, translates to a small total number of analyte molecules. Therefore, local enrichment of the analyte in the detection volume is often desirable. Many methods have been developed to accomplish preconcentration in LoCs.[6] A recent review article summarizes the fundamental principles of BPE focusing and describes its relationship to other concentration enrichment methods.[1] Briefly, BPE focusing falls under the category of electrokinetic

[a]*Department of Chemistry and Biochemistry, Center for Electrochemistry, and the Center for Nano- and Molecular Science and Technology, The University of Texas at Austin, 1 University Station, A5300, Austin, Texas, 78712-0165, USA. E-mail: crooks@cm.utexas.edu*
[b]*Department of Chemistry, Philipps-Universität Marburg, Hans-Meerwein-Strasse, 35032 Marburg, Germany. E-mail: tallarek@staff.uni-marburg.de*

† Electronic supplementary information (ESI) available: In all experiments in which the 8 Au microband electrodes were used, spikes in fluorescence intensity arose due to reflection of the fluorescence from the microbands. Details regarding removal of these spikes from the data are provided. Fluorescence and electric field profiles depicting the collapse of the electric field gradient and loss of the enriched band at excessively high pressure driven flow rates is also included. See DOI: 10.1039/c0lc00351d

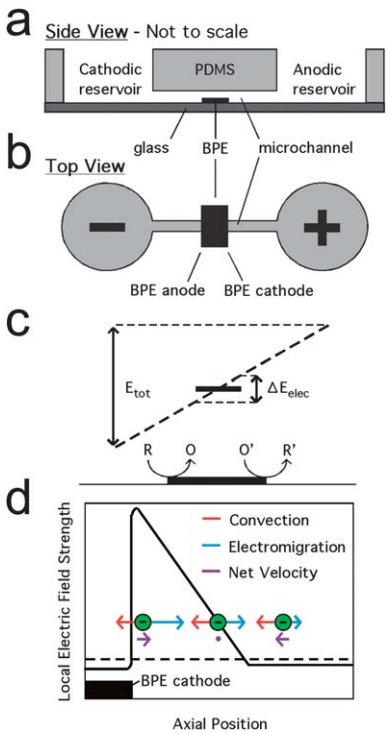

Fig. 1 Schematic (a) side and (b) top views of the hybrid PDMS/glass microdevice used for BPE focusing. A BPE is located at the center of the single, straight microchannel. A driving potential is applied at the anodic and cathodic reservoirs at the ends of the microchannel. (c) Diagram showing the electrical potential (E_{tot}) dropped linearly along the microchannel. The potential dropped along the length of the BPE (ΔE_{elec}) leads to oxidation (R → O) and reduction (O′ → R′) reactions at the ends of the BPEs. (d) Schematic representation of the local axial electric field adjacent to the BPE cathode when the BPE is active (black solid line) and inactive (dashed line). The net velocity vectors are shown at three locations for an anionic species under the combined forces of convection and electromigration.

equilibrium techniques, which also includes isoelectric focusing (IEF),[7–9] field amplified sample stacking,[10,11] isotachoporesis,[12,13] and counter-flow gradient focusing (CFGF) methods.[3,14] BPE focusing is a CFGF method.

CFGF methods balance electromigration velocity against a counterflow. In these methods, there is a gradient in electric field strength along a microchannel, and each analyte is focused at a unique location based on its electrophoretic mobility. Prominent examples include temperature gradient focusing (TGF),[15–18] electric field gradient focusing (EFGF),[19–24] and dynamic field gradient focusing (DFGF).[25–27] A very steep electric field gradient can also form at the boundary of a zone depleted of ions in an electrolyte-filled channel. Such depletion zones can be produced at junctions between micro- and nanoscale channels in a process termed ion concentration polarization (ICP).[28–31] Han and coworkers exploited ICP to focus 33 fM green fluorescent protein 10 million-fold in 35 min (4760-fold per s).[28] The extent and rate of enrichment were found to be highly dependent on initial protein concentration. For example, enrichment fell to 100-fold and a rate of 0.11-fold per s when the initial GFP concentration was increased from 33 fM to 33 nM. Others have observed a similar enrichment dependence on the initial concentration of analyte.[5,32]

Previously we reported enrichment at an ion depletion zone formed by BPE focusing.[1,3–5] In the present report, the relationship between the electric field profile and enrichment behavior in BPE focusing is described, and we present guidelines for tuning the electric field properties to maximize enrichment. Specifically, we demonstrate that the slope of the field gradient increases with the concentration of the buffer, and this in turn leads to a narrower tracer band and more rapid enrichment. Decreasing the flow velocity (cathodic electroosmotic flow (EOF)) in the microchannel through the addition of opposing pressure driven flow extends the ion depletion zone boundary further from the BPE and is accompanied by a corresponding shift of the enriched tracer location. Coating the channel walls with a non-ionic hydrophilic surfactant suppresses bubble formation at the BPE, thereby allowing the use of higher applied voltages and this leads to higher enrichment factors. The wall coating also decreases non-uniform flow and associated Taylor dispersion. Finally, the strength and slope of an electric field gradient are shown to be stable over at least 400 s of continuous enrichment of an anionic fluorescent tracer, and the field strength at the focusing point can be predicted from simple electrokinetic equations.

Experimental section

Chemicals

4,4-Difluoro-1,3,5,7,8-pentamethyl-4-bora-3a,4a-diaza-*s*-indacene-2,6-disulfonic acid (BODIPY^{2-}, Molecular Probes, Eugene, OR) was used as a fluorescent tracer to quantitate the degree of concentration enrichment. Molecular biology grade 1.0 M Tris–HCl buffer (Fisher Biotech, Fair Lawn, NJ) was diluted to concentrations of 1.0, 5.0, or 10.0 mM (pH 8.1) with deionized water (18.0 MΩ cm, Milli-Q Gradient System, Millipore) and used as background electrolyte. The silicone elastomer and curing agent (Sylgard 184) used to prepare the poly (dimethylsiloxane) (PDMS) microfluidic devices were obtained from K. R. Anderson, Inc. (Morgan Hill, CA). Pluronic F108 (ethylene-oxide/propylene-oxide block copolymer) was obtained from BASF (Florham Park, NJ).

Device fabrication

The hybrid PDMS/glass microfluidic devices and Au electrodes were fabricated by a previously published procedure.[33] Briefly, a microfluidic channel (6.0 mm long, 100 μm wide, and ~20 μm high) spanning two 4.0 mm diameter reservoirs was fabricated from PDMS. Next, 100 nm thick Au electrodes (no adhesion layer, Evaporated Metal Films, Ithaca, NY) were microfabricated on glass slides using standard photolithographic techniques. Finally, the PDMS and glass were exposed to an O_2 plasma (60 W, model PDC-32G, Harrick Scientific, Ossining, NY) for 15 s and then bonded together. The BPE was centered at the midpoint of the channel.

Two different electrode configurations were used in this study. For experiments in which enrichment alone was quantified, focusing was carried out using a continuous, 500 μm long BPE that spanned the width of the channel. The BPE used for electric field measurements was of a split design (Fig. 2a). Each half

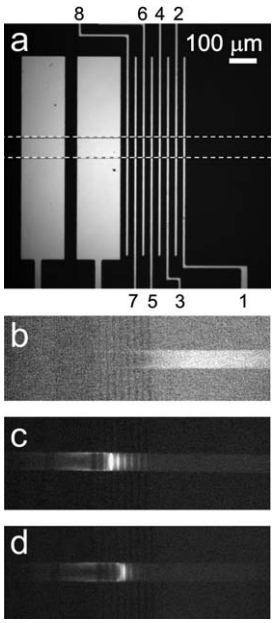

Fig. 2 (a) Optical image of a split Au BPE and 8 Au microband electrodes used for measuring the electric field gradient. The split BPE has a total length of 500 μm and is interrupted by a 50 μm gap. The microbands are ~15 μm wide and are 40 μm on center. All electrodes span the 100 μm wide microchannel (indicated by the dashed white lines). (b–d) Fluorescence micrographs showing enrichment of 100 nM $BODIPY^{2-}$ at $E_{tot} = 35.0$ V in (b) 1.0, (c) 5.0, and (d) 10.0 mM Tris (pH 8.1) with 8.5, 3.5, and 2.5 μL excess buffer solution in the cathodic reservoir, respectively. The images were obtained (b) 1500, (c) 800, and (d) 290 s after enrichment was initiated.

of the BPE was 225 μm long, and there was a 50 μm gap between them. Leads from the two halves of the split BPE extended outside of the microchannel and could be connected externally by a conductive wire so that they acted like a single, 500 μm long BPE.[2,34–36] This design simplified negative control experiments, because the BPE was deactivated when the external connection was removed. To measure the electric field adjacent to the split BPE, 8 microband electrodes (each ~15 μm wide and having a center-to-center distance of 40.0 μm) were situated next to the cathodic pole of the BPE (Fig. 2a). The microband electrodes also extended from beneath the PDMS monolith so they could be connected to a digital multimeter.

Concentration enrichment experiments

Prior to each experiment, the microfluidic channel was rinsed with buffer (1.0, 5.0, or 10.0 mM Tris, pH 8.1) by introducing a solution height differential (~2 mm) between the reservoirs, and allowing the buffer solution to flow through the microchannel for 20 min. Next, the rinsing solution in each of the reservoirs was replaced with 40.0 μL of buffer containing either 5.0 or 100 nM $BODIPY^{2-}$. In some cases, additional microlitre increments of the same solution were added to each reservoir in individual experiments as indicated in the Results and discussion section.

Concentration enrichment experiments were carried out by applying a driving voltage (E_{tot} = 35.0 or 60.0 V) across the microchannel using a high-voltage power supply (LLS9120, TDK-Lambda Americas, Inc., San Diego, CA) connected to the microfabricated Au driving electrodes spanning the bottoms of the reservoirs. Simultaneously, the extent of enrichment was monitored by fluorescence microscopy.

Fluorescence measurements

Enrichment of the $BODIPY^{2-}$ tracer dye was monitored using a fluorescence microscope (Multizoom AZ100, Nikon, Japan) fitted with a CCD camera (QuantEM 512SC, Photometrics, Tucson, AZ, USA). Images were recorded at 1 s intervals by a CCD camera and analyzed by image processing software. The enrichment factor was calculated by dividing the maximum concentration in the focused tracer band by the initial tracer concentration. Values of the enrichment factor were determined by comparing the region of maximum intensity in the concentrated band of dye to calibrated fluorescence intensities. Intensity traces showing the band profile along the channel length were obtained by averaging the fluorescence intensity across the middle 70 μm of the 100 μm wide microchannel. All measurements were corrected for the background fluorescence intensity.

Electric field monitoring

The axial electric field profile was monitored using a scanning digital multimeter (SDMM, Model 2700, Keithley Instruments, Inc., Cleveland, OH) equipped with a multiplexer module (Model 7701, Keithley) and connected to the 8 microband electrodes described in the previous subsection. The SDMM was controlled in Microsoft Excel *via* the software provided by the SDMM manufacturer (ExceLinx, Keithley). The SDMM was interfaced to the microband electrodes through a breakout board (screw terminals). The SDMM reads the difference between the two microbands farthest from the BPE first ($\Delta E_{1,2}$, Fig. 2a), and then sequentially measures the potential between the second and third microbands ($\Delta E_{2,3}$) and so forth until the last pair ($\Delta E_{7,8}$) is reached. The acquisition time for each voltage measurement was ~0.1 s, and the voltage between pairs of microbands was read every 2 s. Electric field monitoring experiments proceeded as follows. First, the two halves of the BPE were connected *via* a conductive wire. Second, the SDMM was placed in scan mode. Third, a driving voltage (E_{tot} = 35.0 or 60.0 V) was applied across the microchannel *via* the driving electrodes. Scans were stored and plotted in real-time in Excel.

Results and discussion

Electric field profile measurements

The local axial electric field strength in a microchannel can be visualized by recording the potential difference between neighboring pairs of Au microband electrodes fabricated on the bottom of the microchannel (Fig. 2a). If the two halves of the split BPE are not connected, and $E_{tot} = 35.0$ V, then the calculated electric field strength throughout the microchannel is $V_m = 5.8$ kV m^{-1}. If the two halves of the BPE are connected, then the resulting ΔE_{elec} ($\Delta E_{elec} \approx E_{tot}(l_{elec}/l_{channel}) = 2.9$ V, where l_{elec} is the length of the BPE, and $l_{channel}$ is the length of the microchannel) is sufficient to initiate the coupled faradaic reactions

given in eqn (1) and (2) at the anodic and cathodic poles, respectively.[2,5] This results in formation of an electric field gradient having the general characteristics of the solid line in Fig. 1d.

$$2H_2O - 4e^- \rightarrow O_2 + 4H^+;\ E^o = 0.40\ V \quad (1)$$

$$2H_2O + 2e^- \rightarrow H_2 + 2OH^-;\ E^o = -0.83\ V \quad (2)$$

$$TrisH^+ + OH^- \rightarrow Tris + H_2O \quad (3)$$

A consequence of the electrochemical reactions taking place at the BPE is that OH^- generated at the cathodic pole neutralizes $TrisH^+$ (eqn (3)).[2,5] This results in a low conductivity zone near the cathodic pole of the BPE that is depleted of buffer cations, and therefore the local electric field in this region increases (Fig. 1d). Buffer anions migrate through this high-field, depletion zone faster than elsewhere in the channel, and therefore the concentration of Cl^- in the depletion zone decreases too.[2,5] The resulting enhanced electric field is observed to have a gradient shape, and it is this gradient that is measured in our experiments. During an experiment, as an anion (such as $BODIPY^{2-}$) is carried from the anodic toward the cathodic reservoir by electroosmotic flow (EOF), its average axial transport velocity is the sum of its mean velocity due to convection (u_m) and opposing electromigration (u_{ep}). As the molecule approaches the cathodic edge of the BPE, it encounters an increasing electric field strength, resulting in increased anodic u_{ep}. The molecule slows, ultimately focusing at a location where $u_m = -u_{ep}$ (Fig. 1d). Focusing behavior at the split BPE (Fig. 2a) has been shown to be similar to that observed at a continuous BPE,[2] and typical enriched bands formed in 1.0, 5.0, and 10 mM Tris buffer are shown in Fig. 2b–d.

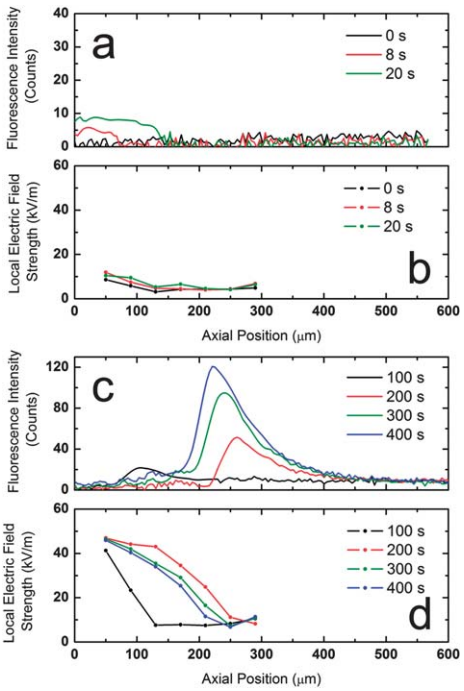

Fig. 3 (a and c) Background-subtracted fluorescence intensity as a function of position along the microfluidic channel (axial position = 0 at the cathodic edge of the BPE). (b and d) Local axial electric field strength as a function of position. The microchannel was filled with 5.0 mM Tris (pH 8.1) containing 100 nM $BODIPY^{2-}$ and E_{tot} = 35.0 V. Pressure-driven flow was initiated by adding 4.0 μL of excess solution to the cathodic reservoir. Fluorescence and electric field profiles were collected every 1 s and 2 s, respectively, and selected time points are shown here to illustrate the evolution of the field on the (a and b) short time scale (0, 8, and 20 s), and (c and d) long time scale (100–400 s). The electrode arrangement shown in Fig. 2a was used for these experiments.

Temporal evolution of the electric field gradient

This subsection describes the formation of the electric field gradient and the subsequent enrichment of the anionic fluorescent tracer $BODIPY^{2-}$. The experiments were carried out as follows using the electrode design shown in Fig. 2a. First, the reservoirs were filled with 40.0 μL of 5.0 mM Tris (pH 8.1) containing 100 nM $BODIPY^{2-}$. An additional 4.0 μL of the same solution was pipetted into the cathodic reservoir. This additional volume adjusts the flow in the microchannel to an optimal rate for enrichment in 5.0 mM Tris. Specifically, it ensures that enrichment begins within 10 s after application of the driving voltage and that the electric field gradient remains stable over time. Second, the two halves of the BPE were connected. Finally, a driving voltage (E_{tot} = 35.0 V) was applied to initiate enrichment.

Fig. 3a and c show the location of the enriched tracer band upon application of the driving voltage on short and long time scales, respectively. Corresponding measured electric field profiles are provided in Fig. 3b and d. Fig. 3a reveals a slight enrichment of the tracer near the cathodic edge of the BPE (axial position = 0). During this initial stage of enrichment, the electric field gradient responsible for enrichment is not detectable (Fig. 3b). This is because the depletion zone has not yet extended from the BPE cathode into the region monitored by the microbands. As shown in Fig. 3c and d, an increase in field strength is first clearly observed at t = 100 s between the two pairs of microband electrodes closest to the BPE edge ($\Delta E_{7,8}$ and $\Delta E_{6,7}$). In Fig. 3d, these positions are 50 μm and 90 μm away from the edge of the BPE, respectively. This evolving gradient in the field corresponds to a small peak in fluorescence intensity centered at ~100 μm (Fig. 3c). Between 100 and 200 s the depleted ion region grows, the electric field gradient extends closer to the anodic reservoir, and the tracer band moves away from the BPE. The field gradient and the location of the enriched band begin to stabilize at t > 200 s, but both the height and width of the tracer peak continue to increase. Both of these peak characteristics are a consequence of $BODIPY^{2-}$ enrichment. That is, as the ionic strength in the region of $BODIPY^{2-}$ enrichment increases, the electric field gradient is reduced.[5] This latter point is important, because it suggests this focusing method will be most effective for low concentrations of analytes. It also implies that there is an upper limit to the local concentration of enriched tracer under a given set of conditions, which include the applied field strength and the ionic strength of the buffer.

As discussed earlier, the centroid of the tracer band is located at the lateral position where $u_m = -u_{ep}$ (Fig. 1d). Its position can be attributed to the *local* electric field strength (V_l) at the focusing

point, which is observed to be ~10 kV m^{-1} in this particular experiment. In the following calculation, this observed value will be compared with the theoretical value. Given the experimentally determined electrophoretic mobility, $\mu_{ep} = (-4.2 \pm 0.2) \times 10^{-4}$ $cm^2\ V^{-1}\ s^{-1}$,[4] eqn (4) can be used to calculate that $u_{ep} = (-4.2 \pm 0.2) \times 10^{-2}$ cm s^{-1} for $BODIPY^{2-}$ when $V_l = 10$ kV m^{-1}.

$$u_{ep} = \mu_{ep} V_l \quad (4)$$

The convective fluid velocity, u_m, can be approximated by measuring the electroosmotic velocity (u_{eo}) and subtracting the average velocity due to the opposing pressure driven flow. Recall that pressure driven flow was introduced by adding 4.0 μL of solution to the cathodic reservoir. The experimentally determined value of u_{eo} is $(4.1 \pm 0.2) \times 10^{-2}$ cm s^{-1}. Numerical simulation indicates that the addition of 4.0 μL of solution to the cathodic reservoir reduces the average flow velocity by only 0.17×10^{-2} cm s^{-1}. Therefore, the calculated value of u_m ($(3.9 \pm 0.2) \times 10^{-2}$ cm s^{-1}) is approximately equal and opposite in sign to the value of u_{ep} ($(-4.2 \pm 0.2) \times 10^{-2}$ cm s^{-1}) when the experimentally determined $V_l = 10$ kV m^{-1} at the focusing point.

It should be noted that the value of the electroosmotic velocity (u_{eo}) used in the foregoing discussion was measured in a channel containing a BPE and corresponds to an electroosmotic mobility (μ_{eo}) that is higher than that reported previously for a PDMS/glass microchannel under similar conditions. For instance, Hellmich *et al.* reported $\mu_{eo} = (2.3 \pm 0.04) \times 10^{-4}$ $cm^2\ V^{-1}\ s^{-1}$ for 20.0 mM phosphate buffer (pH 8.2) in a hybrid PDMS/glass device which had been treated with an O_2 plasma prior to assembly in a manner similar to the devices used in our study.[37] The value of μ_{eo} can be calculated from the measured u_{eo} using the relationship given in eqn (5).

$$\mu_{eo} = \frac{u_{eo}}{V_m} \quad (5)$$

Here V_m is the *mean* electric field strength (5.8 kV m^{-1}), which is used because variations in the local electric field, V_l (and associated u_{eo} values), along the channel are mitigated by mass conservation in incompressible fluid flow and effectively averaged. The calculated value of μ_{eo} is $(7.1 \pm 0.4) \times 10^{-4}$ $cm^2\ V^{-1}\ s^{-1}$ in the presence of a BPE, which is significantly larger than the value we measure in the absence of a BPE ($\mu_{eo} = (5.3 \pm 0.4) \times 10^{-4}$ $cm^2\ V^{-1}\ s^{-1}$) under similar conditions. This finding will be discussed in more detail later, but briefly, the increased apparent electroosmotic mobility is observed only in the presence of a BPE and is due to the formation of the ion depletion zone. The local mobility ($\mu_{eo,l}$) is much higher in this zone due to the decreased ionic strength.[38–40] The locally high mobility increases the average fluid flow velocity in the entire channel causing the measured u_{eo} and apparent μ_{eo} to be higher than expected.

Effects of buffer concentration and flow rate

The electric field gradient can be manipulated by exerting control over the experimental conditions. For example, the effect of Tris buffer concentration and flow rate on the field gradient are illustrated by the results shown in Fig. 4. These two variables are considered together, because enrichment for each buffer concentration is optimized at a different convective flow rate.

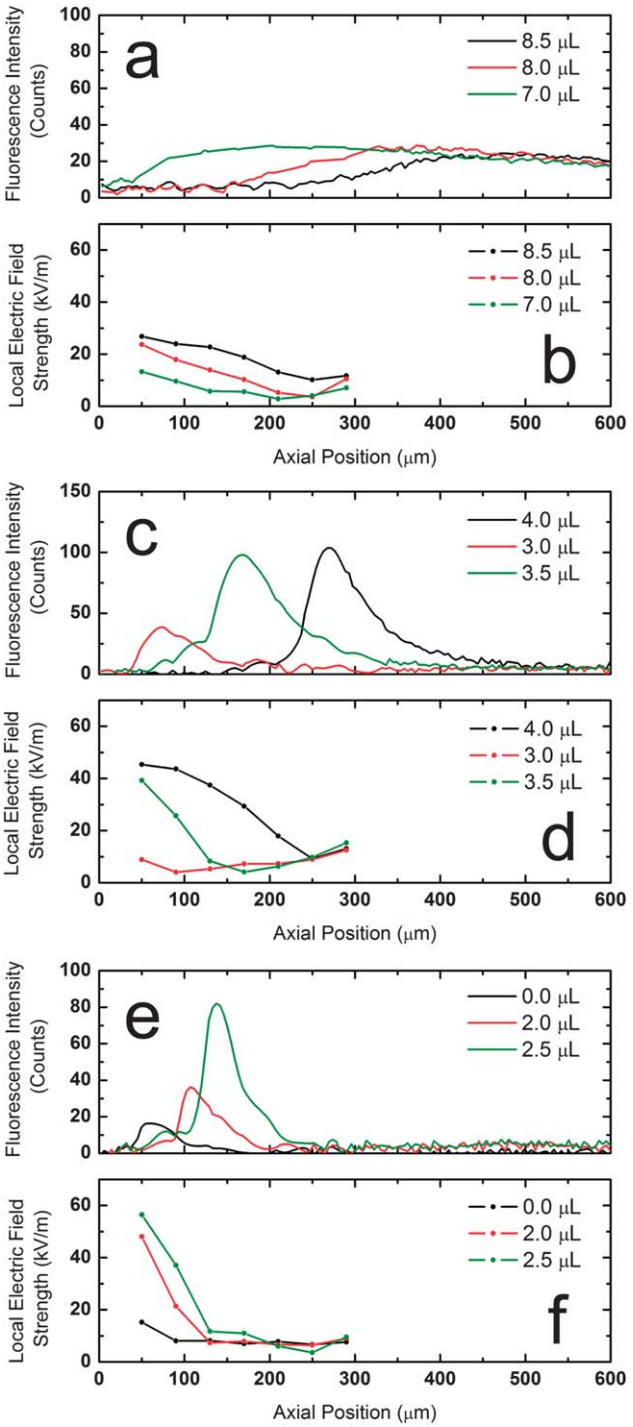

Fig. 4 (a, c, and e) Background-subtracted fluorescence intensity as a function of position along the microfluidic channel (axial position = 0 at the cathodic edge of the BPE). (b, d, and f) Local axial electric field strength as a function of position. The microchannel was filled with 100 nM $BODIPY^{2-}$ plus (a and b) 1.0 mM, (c and d) 5.0 mM, and (e and f) 10.0 mM Tris (pH 8.1). Pressure-driven flow was initiated by adding the indicated volumes of excess solution to the cathodic reservoir. Fluorescence and electric field profiles were collected every 1 s and 2 s, respectively. The electrode arrangement shown in Fig. 2a was used for these experiments. $E_{tot} = 35.0$ V.

These experiments were carried out as follows. First, 40.0 μL of Tris buffer (1.0, 5.0, or 10.0 mM, pH 8.1) containing 100 nM $BODIPY^{2-}$ was added to each reservoir. Second, the BPE halves were connected. Third, $E_{tot} = 35.0$ V ($V_m = 5.8$ kV m^{-1}) was applied to initiate enrichment. Simultaneously, the fluorescence intensity and electric field profiles were recorded.

Fig. 4a shows fluorescence intensity profiles obtained during enrichment of 100 nM fluorescent tracer in 1.0 mM Tris. In this experiment, enrichment did not begin immediately, but rather it was induced by addition of 8.0 μL of buffer/$BODIPY^{2-}$ solution to the cathodic reservoir. After enrichment began, the volume in the cathodic reservoir was increased and decreased multiple times in 0.5, 1.0, or 2.0 μL increments to change the position of the enriched band. These volume additions and removals were randomized to decouple total enrichment time from band position. Fig. 4a shows fluorescence profiles for tracer enriched in 1.0 mM Tris with excess volumes of 8.5, 8.0, and 7.0 μL in the cathodic reservoir. These steps are reported in chronological order during a sequence in which volume was being removed in 0.5 μL increments. For each removal of 0.5 μL from the 4.0 mm diameter cathodic reservoir, the solution height decreases by 0.04 mm, which is estimated by numerical simulations to increase the flow velocity (towards the cathodic reservoir) by 2.1×10^{-4} cm s^{-1}. As seen in Fig. 4a, although this change is small, its effect on the position of the enriched band is marked. When a greater excess volume is present in the cathodic reservoir (on the left-hand side with respect to Fig. 4a), the enriched band is located further from the BPE (*i.e.*, to the right). Note that although 8.0 μL excess volume in the cathodic reservoir was required to initiate enrichment, the focused band was maintained with an excess volume of just 7.0 μL.

The local electric field strength corresponding to the data in Fig. 4a is plotted in Fig. 4b. The most notable characteristics of these field gradients are that they have both low magnitudes and shallow slopes, which correlate to the broad, low-intensity tracer bands. The specific positions of the enriched tracer bands also correlate to the shape of the field gradients. Specifically, enrichment is excluded from regions in which V_l is $>\sim$10 kV m^{-1}. Note that the measured value of u_{eo} for 1.0 mM Tris (pH 8.1) in the presence of a BPE is 5.1×10^{-2} cm s^{-1}. The decrease in average linear flow velocity resulting from 8.0 μL excess solution in the cathodic reservoir is estimated to be 0.34×10^{-2} cm s^{-1}. Under these conditions, the band is expected to form at $V_l = 11.6$ kV m^{-1} based on eqn (4).

In contrast to the enrichment behavior observed for 1.0 mM buffer, the fluorescence line profiles for 5.0 mM Tris (Fig. 4c) exhibit better-defined peaks. In this case, the experiment was initiated with 4.0 μL of excess solution in the cathodic reservoir, and this resulted in formation of an enriched band centered at $\sim$270 μm to the right of the BPE edge. Next, 1.0 μL was removed from the cathodic reservoir (3.0 μL total excess), which resulted in the enriched band shifting toward the BPE. During this adjustment, the degree of enrichment decreased. This loss of fluorescence intensity is a consequence of leakage of the tracer over the BPE and toward the cathodic reservoir. That is, some of the tracer escapes from the concentrated band as it nears the edge of the BPE. Finally, 0.5 μL of buffer solution was added to the cathodic reservoir (3.5 μL total excess) restoring the band to an intermediate position. The fluorescence intensity profile shown in Fig. 4c was obtained 100 s after addition of the buffer, and during this period it re-enriched to nearly the level observed with 4.0 μL excess buffer present.

Fig. 4d demonstrates a locally enhanced maximum electric field ($V_{l,max}/V_m \approx 7$) in 5.0 mM Tris with the field strength exceeding 40 kV m^{-1} close to the BPE. Because the field gradient is steep, the tracer band is narrower compared to those observed for 1.0 mM Tris. Comparison of the location of the peak fluorescence intensity with the electric field profile at 3.5 μL excess solution (Fig. 4c and d) reveals that the enriched band is focused in a region where $V_l \approx 10$ kV m^{-1}. Under these conditions, the theoretical value of the field strength at the focusing location is $V_l = 9.6$ kV m^{-1}.

Finally, the data shown in Fig. 4e and f, obtained in 10.0 mM Tris buffer, show a continuation of the trends described for the two lower concentrations. In this experiment, enrichment began immediately (no addition of buffer to the cathodic reservoir required) when $E_{tot} = 35.0$ V (Fig. 4e). Once enrichment began, aliquots of 2.0 μL and then an additional 0.5 μL of buffer were added to the cathodic reservoir. This resulted in the enriched band moving to the right, and becoming more intense and narrower. The narrowness and location of the tracer bands (Fig. 4e) correlate well with the steep slope and positioning of the electric field gradient (Fig. 4f). Again, the band is focused at a location for which $V_l \approx 10$ kV m^{-1}. Note that the calculated value of V_l at the focusing location is 9.0 kV m^{-1} (based on the measured $u_{eo} = 3.7 \times 10^{-2}$ cm s^{-1}) when no pressure driven flow is added. The close correspondence between the measured and theoretical V_l values for all three Tris buffer concentrations provides confidence in the model embodied by Fig. 1d.

It is important to examine the underlying principles responsible for the trends in the data presented in Fig. 4. The first notable trend is that the slope of the field gradient is directly related to the concentration of the Tris buffer (Fig. 4b, d and f). This is because at higher concentrations, OH^- produced at the cathodic edge of the BPE reacts quickly, resulting in a narrow ion-depletion zone. For this reason, the tracer bands form close to the BPE in 10.0 mM Tris. Furthermore, the difference in conductivity in the depletion zone and elsewhere in the channel is greater in 10.0 mM Tris than at lower buffer concentrations. Taken together with the narrowness of the depletion zone, this difference in conductivity results in high local electric field strength (up to nearly 60 kV m^{-1}, $V_{l,max}/V_m \approx 10$). Perhaps the obvious question is why all enrichment experiments are not carried out in 10.0 mM Tris buffer (or even higher). The disadvantage of higher buffer concentration is that it increases the faradaic current at the BPE, leading to more rapid production of gas (eqn (1) and (2)), and hence bubbles at the BPE.[1]

The second trend is that the amount of excess volume required in the cathodic reservoir to optimize enrichment during a given experiment is lower at higher buffer concentrations. This is because the excess volume slows the flow rate, and at high buffer concentrations, the EOF is already slower due to a decrease in ζ potential at the microchannel walls. Therefore, the EOF alone is already optimal for enrichment. Furthermore, if too much excess volume is added to the cathodic reservoir during enrichment in 10.0 mM Tris, the electric field gradient collapses and the enriched band dissipates (see ESI†).

Quantitation of enrichment factor as a function of buffer concentration

Fig. 5a shows typical enrichment factors (EFs) achieved within the first 900 s after applying $E_{tot} = 35.0$ V across unmodified (no Pluronic, *vide infra*) PDMS/glass microchannels containing 1.0, 5.0, and 10.0 mM Tris and 100 nM $BODIPY^{2-}$. These data were obtained using a microchannel having a continuous 500 μm BPE situated at the center and no microband electrodes. This simplified design is ideal for determination of EFs, because otherwise reflection of the tracer fluorescence from microband electrodes interferes with the analysis. To obtain EFs, the reservoirs are first filled with 40.0 μL of Tris buffer solution containing the $BODIPY^{2-}$ tracer. The 1.0, 5.0, and 10.0 mM Tris enrichment experiments began with 8.0, 4.0, and 0.0 μL of excess volume in the cathodic reservoir, respectively, to optimize and stabilize the enriched band. Second, $E_{tot} = 35.0$ V was applied across the microchannel, and the subsequent enrichment of the tracer was monitored by fluorescence microscopy. EFs were determined by comparing the maximum fluorescence intensity in the enriched band to calibration curves of fluorescence intensity *versus* tracer concentration.

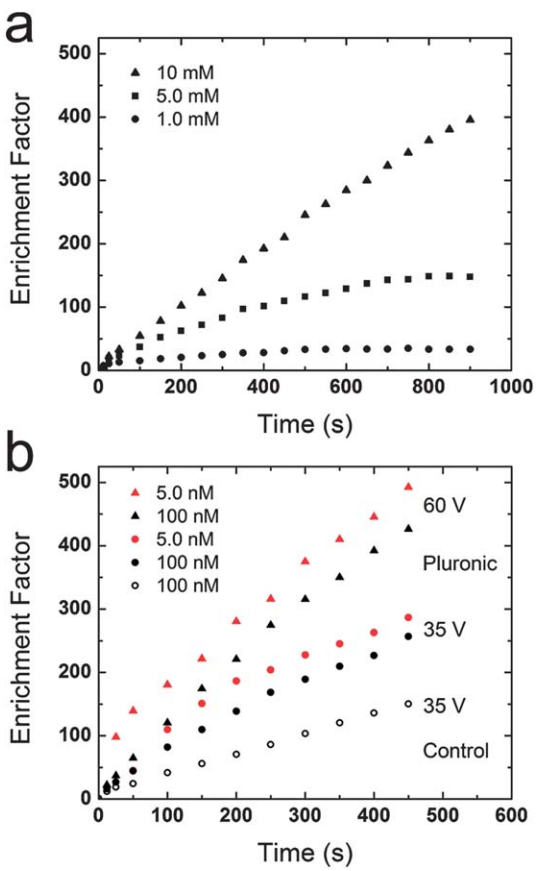

Fig. 5 Plot of enrichment factor *vs.* time. (a) The enrichment experiments were carried out using solutions containing 100 nM $BODIPY^{2-}$ and 1.0, 5.0, or 10.0 mM Tris (pH 8.1). Pressure-driven flow was initiated by adding 8.0, 4.0, and 0 μL, respectively, of excess solution to the cathodic reservoirs. $E_{tot} = 35.0$ V. (b) The enrichment experiments were carried out in microchannels modified with Pluronic (see main text) and using solutions containing 5.0 mM Tris (pH 8.1) and either 5.0 or 100 nM $BODIPY^{2-}$. $E_{tot} = 35.0$ or 60.0 V as indicated in the figure. No pressure-driven flow was required to initiate concentration enrichment. The control experiment was identical to the others carried out at $E_{tot} = 35.0$ V, but the channel was not modified with Pluronic. The 500 μm split BPE (no microband electrodes) was used for this experiment.

The results in Fig. 5a show that enrichment proceeds more rapidly as the Tris concentration is increased. The rate of enrichment from $t = 25$ s to 300 s is linear for 1.0, 5.0, and 10.0 mM Tris and is measured to be 0.05-fold per s, 0.23-fold per s, and 0.46-fold per s, respectively. The maximum EF also increases with buffer concentration. The maximum enrichments achieved in 1.0 mM and 5.0 mM Tris were 33-fold and 145-fold, respectively. The EF did not plateau in 10.0 mM Tris and continued to increase past 400-fold at 900 s. To understand these results, recall that the enhancement of the electric field in the depleted-ion region is caused by a disparity in conductivity between the ion-depletion region and the rest of the channel. The magnitude of the field enhancement ($V_{l,max}/V_m$) is proportional to the ratio of the conductivities inside and outside the depletion region. This ratio is larger at higher buffer concentration. For instance, $V_{l,max}/V_m \approx 7$ and 10 for 5.0 and 10.0 mM Tris, respectively (Fig. 4). Furthermore, as the local concentration of $BODIPY^{2-}$ increases, it augments the local ionic strength, which, as we have already discussed, negatively impacts the slope of the electric field gradient. That is, when the enriched band concentrates sufficiently, the boundary between the depletion zone and the buffer becomes less distinct and a maximum EF obtains. This causes the EF-*versus*-time plot (Fig. 5a) to plateau. The effect of this enrichment saturation is two-fold. First, as already mentioned, the maximum achievable EF is higher for higher buffer concentrations. Second, for a given buffer concentration, a lower initial tracer concentration results in higher enrichment. We have reported and discussed this trend previously.[5] Higher EFs for analytes initially present at lower concentrations was also observed by Han and coworkers.[28] Though they did not address this trend, it was pointed out subsequently by Shackman and Ross.[14]

Enrichment in a microchannel coated with a neutral surfactant and at a higher driving voltage (E_{tot})

Previously, we reported enhanced enrichment of 100 nM $BODIPY^{2-}$ (~600-fold in 200 s, 3-fold per s) during separation experiments when the microchannel was coated with the neutral block copolymer Pluronic.[4] In this subsection, we compare enrichment in coated and uncoated microchannels, and correlate the EF to the electric field characteristics. The enrichment of $BODIPY^{2-}$ in a Pluronic-coated microchannel is shown in Fig. 5b. In these experiments, the channel walls were coated by introducing a 3.0 μM solution of Pluronic in 10.0 mM Tris (pH 8.1) and allowing it to stand for 20 h. As a control, a second microchannel was similarly filled with Pluronic-free buffer solution. After coating, the microchannels were thoroughly rinsed with 5.0 mM Tris (pH 8.1) by introducing a ~2 mm height differential between the reservoirs and allowing the solution to flow for 5 min. This was repeated once more with fresh buffer. Next, the reservoirs were emptied, and then 40.0 μL of 5.0 mM Tris (pH 8.1) containing 5.0 or 100 nM $BODIPY^{2-}$ was added to

each reservoir. Finally, a driving voltage was applied across the channel to initiate enrichment (E_{tot} = 35.0 or 60.0 V).

The resulting EF *versus* time plots (Fig. 5b) have three distinct characteristics. First, under all conditions, a slightly higher enrichment factor was achieved with the lower $BODIPY^{2-}$ concentration. Second, for a particular set of experimental conditions, enrichment occurs more rapidly in the coated channels. This point will be discussed in more detail in the next subsection. Third, bubble formation at the BPE is suppressed in the Pluronic-coated channels, and therefore it is possible to use higher values of E_{tot} which lead to higher EFs. As discussed later, this enhancement is attributed to a steeper electric field gradient and faster transport of the tracer to the enrichment zone. For example, Pluronic coating alone increases the rate of enrichment of 100 nM $BODIPY^{2-}$ from 0.36-fold per s to 0.57-fold per s, reaching over 250-fold enrichment in 450 s. Increasing the driving voltage to E_{tot} = 60.0 V brings the enrichment rate to 0.96-fold per s, nearing 450-fold in 450 s.

Electric field profile measurements in a microchannel coated with a neutral surfactant (E_{tot} = 35.0 and 60.0 V)

Here we describe the nature of the electric field profile in Pluronic-coated channels. These measurements were carried out exactly as described for the uncoated channels. Briefly, the electroosmotic mobility of the buffer solution was suppressed by coating the PDMS microchannels with Pluronic as described in the previous subsection. Second, the microchannel reservoirs were each filled with 40.0 μL of 100 nM $BODIPY^{2-}$ in 5.0 mM Tris (no pressure-driven flow). Third, the two halves of the BPE were connected *via* a conductive wire. Fourth, the SDMM was activated to scan the potential difference between neighboring microband electrodes. Finally, E_{tot} = 35.0 or 60.0 V was applied across the channel to initiate enrichment.

Fig. 6a and b show the fluorescence intensity traces and corresponding electric field profiles, respectively, obtained during a typical enrichment of 100 nM $BODIPY^{2-}$ in 5.0 mM Tris at E_{tot} = 35.0 V. Comparison of this enrichment behavior with that shown in Fig. 3c and d under the same conditions, but in an uncoated channel, reveals three important characteristics. First, no pressure-driven flow is required to reach conditions appropriate for enrichment, which is consistent with the fact that the electroosmotic flow velocity is slower in a Pluronic-coated channel. Second, the enrichment of the dye is significantly enhanced in the coated channel: within 400 s of applying E_{tot}, the EF is ~180 *versus* ~75 in the uncoated channel. Third, the electric field profile is not markedly different in the coated and uncoated channels, having a similar maximum value of ~50 kV m^{-1} and extending 250–300 μm to the right of the BPE.

Despite the presence of similar electric field gradients in coated and uncoated channels at E_{tot} = 35.0 V, enrichment is significantly enhanced in the coated channels. This can be attributed to a reduction in electroosmotic mobility differentials along the channel. As mentioned earlier, the width of the enriched band is determined mainly by the steepness of the electric field, but it can be greatly increased by Taylor dispersion. The electroosmotic velocity in the ion-depleted region ($u_{eo,l}$) is significantly increased due to *both* the enhanced electric field and the low ionic strength, which results in increased ζ potential at the channel walls. If the

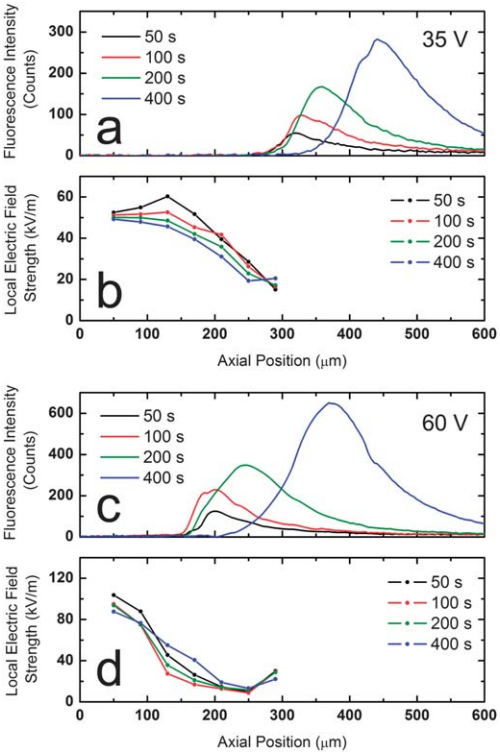

Fig. 6 Evolution of the (a and c) background-subtracted fluorescence intensities and (b and d) local axial electric field strengths as a function of time in the absence of pressure-driven flow. The walls of the microchannel were coated with Pluronic, and the channel was filled with a solution containing 5.0 mM Tris (pH 8.1) and 100 nM $BODIPY^{2-}$. (a and b) E_{tot} = 35.0 V and (c and d) E_{tot} = 60.0 V. The axial position = 0 at the cathodic edge of the BPE. The electrode configuration shown in Fig. 2a was used for these experiments.

driving force for EOF in the depletion zone becomes significantly greater than in neighboring channel segments, parabolic backflow, and even vortex flow, can develop.[31,38,39] The band broadening due to these phenomena is worse than Taylor dispersion arising from simple laminar flow.[40] Maynes *et al.* derived a useful relationship (eqn (6)) for estimating the width of a peak focused along an electric field gradient when taking electroosmotic velocity differentials into account.[40]

$$s = \sqrt{\frac{D_{im} + \left(\frac{u_{eo,l}}{u_m} - 1\right)^2 \frac{a^2 u_m^2}{52.5 D_{im}}}{|\mu_{ep} m|}} \quad (6)$$

Here s is the standard deviation of the width of a focused band, D_{im} the diffusion coefficient of the focused species, a the half-height of a 2-D (parallel plate) rectangular channel, and m the local slope of the electric field gradient.[40] Importantly, in the absence of electroosmotic velocity differentials ($u_{eo,l} = u_m$) eqn (6) simplifies to include only three parameters determining the peak width: the molecular diffusivity (D_{im}), the electrophoretic mobility (μ_{ep}), and the electric field gradient slope (m). Note that, in this case of uniform flow, a steeper slope of the electric field gradient is the only experimental variable (related to Taylor dispersion) providing access to improved enrichment. More

significantly, eqn (6) suggests two possible solutions for limiting dispersion induced by the non-uniform EOF. Taylor dispersion will lessen with suppression of the EOF (decreasing $u_{eo,l}$) while maintaining the same u_m, or with a reduction in channel dimensions (a).

This mathematical treatment (eqn (6)) explains the enhanced enrichment observed in Pluronic coated channels. The coating protocol used here[4] suppresses the EOF by decreasing the wall charge. To understand this enhancement, consider the limiting case in which the charge on the channel walls is zero, and all flow (u_m) is pressure driven. In this case, variations in ionic strength and V_l along the channel will no longer have an adverse effect on the uniformity of flow.

Finally, we consider the effect of increasing E_{tot} on the enrichment process. Fig. 6c and d show the outcome of an experiment conducted under the same conditions used to obtain the results shown in Fig. 6a and b, but here $E_{tot} = 60.0$ V. As before, no pressure-driven flow was used. Two important comparisons may be made between the results obtained at $E_{tot} =$ 35.0 and 60.0 V. First, the extent of enrichment at 400 s increased from EF ~180 to ~410. Second, the maximum field strength and the slope of the gradient are both increased at the higher value of E_{tot}. At $E_{tot} = 35.0$ V the maximum field strength measured at $t =$ 400 s is ~48.0 kV m^{-1} and the slope of the gradient is 1.50×10^5 kV m^{-2}. By comparison, at $E_{tot} = 60.0$ V ($t = 400$ s), these quantities are ~87 kV m^{-1} and 4.18×10^5 kV m^{-2}.

There are three reasons for the improvement in EF at higher values of E_{tot}. First, transport of the tracer to the focusing zone is faster. Recall that the dominance of convective flow (driven by EOF) over electromigration is responsible for moving the tracer from the anodic reservoir to the focusing location. Therefore, it is necessary that $\mu_{eo} > \mu_{ep}$. The corresponding dominance of electroosmotic over electrophoretic velocity ($u_{eo} > u_{ep}$) between the anodic reservoir and focusing location is magnified at higher field strengths, resulting in faster enrichment. Second, the electric field gradient is steeper. This may be due to higher faradaic current passing through the BPE leading to faster production of OH^- and subsequent neutralization of $TrisH^+$. A steeper field gradient signifies a sharper transition in ionic strength inside and outside the depletion zone. A third reason for enhanced enrichment is the increase of both sequestering forces, convection (u_{eo}) and opposing electromigration (u_{ep}) of the tracer, at the focusing location at higher E_{tot}.

Conclusions

In conclusion, we have reported simultaneous measurements of the evolution of the electric field gradient and an enriched tracer band during BPE focusing. These studies have provided insight into the factors affecting the location of the band and extent of enrichment. We also correlated the location of the band to the position of the field gradient and the specific local electric field strength at which the convective and electrophoretic velocities of the tracer balanced. These findings make it possible to tune the slope of the electric field gradient and its position by modulating the concentration of the buffer, the flow velocity, and the applied electric field strength. More rapid enrichment is achieved at higher buffer concentrations and higher applied fields, both of which increase the slope of the electric field gradient. Coating the channel with the neutral surfactant Pluronic does not have a significant impact on the magnitude or slope of the electric field gradient, but nevertheless the coated channels lead to a significant increase in enrichment rate. This enhancement is understood to be the result of decreased Taylor dispersion. Specifically, the neutral coating suppresses non-uniform EOFs throughout the channel.

Ongoing research focuses on using the findings reported here to achieve even greater enrichment of individual species and improved separation of solutions containing multiple analytes. Measurements of the electric field gradient during separation experiments will be especially interesting, because our previous studies indicated that mixed analytes concentrate in different locations compared to the individual components.[4] This finding implies a complex and dynamic electric field profile in the case of mixed analytes. The results of these new experiments will be reported in due course.

Major symbols

a	half height of a rectangular channel, m
D_{im}	molecular diffusivity, m^2 s^{-1}
ΔE_{elec}	potential difference between two ends of the bipolar electrode, V
E^o	standard reduction potential, V
$\Delta E_{n,m}$	potential difference between microband electrodes n and m, V
E_{tot}	applied voltage between the driving electrodes, V
$l_{channel}$	length of the microchannel, m
l_{elec}	length of the bipolar electrode, m
m	slope of the electric field gradient, kV m^{-2}
μ_{eo}	electroosmotic mobility, cm^2 V^{-1} s^{-1}
$\mu_{eo,l}$	local electroosmotic mobility, cm^2 V^{-1} s^{-1}
μ_{ep}	electrophoretic mobility, cm^2 V^{-1} s^{-1}
s	standard deviation of the width of a focused band, m
u_{eo}	electroosmotic velocity, cm s^{-1}
$u_{eo,l}$	local electroosmotic velocity, cm s^{-1}
u_{ep}	electrophoretic velocity, cm s^{-1}
u_m	mean convective flow velocity, cm s^{-1}
V_l	local electric field strength, kV m^{-1}
$V_{l,max}$	maximum measured local electric field strength, kV m^{-1}
V_m	mean electric field strength, kV m^{-1}

Acknowledgements

We gratefully acknowledge support from the Chemical Sciences, Geosciences, and Biosciences Division, Office of Basic Energy Sciences, Office of Science, US Department of Energy (Contract No. DE-FG02-06ER15758). We also thank the Robert A. Welch Foundation (Grant F-0032) for sustained support. This material is based in part upon work supported under a National Science Foundation Graduate Research Fellowship awarded to RKA.

Notes and references

1 F. Mavré, R. K. Anand, D. R. Laws, K.-F. Chow, B.-Y. Chang, J. A. Crooks and R. M. Crooks, *Anal. Chem.*, 2010, **82**, 8766–8774.
2 R. K. Perdue, D. R. Laws, D. Hlushkou, U. Tallarek and R. M. Crooks, *Anal. Chem.*, 2009, **81**, 10149.
3 R. Dhopeshwarkar, D. Hlushkou, M. Nguyen, U. Tallarek and R. M. Crooks, *J. Am. Chem. Soc.*, 2008, **130**, 10480.
4 D. R. Laws, D. Hlushkou, R. K. Perdue, U. Tallarek and R. M. Crooks, *Anal. Chem.*, 2009, **81**, 8923.
5 D. Hlushkou, R. K. Perdue, R. Dhopeshwarkar, R. M. Crooks and U. Tallarek, *Lab Chip*, 2009, **9**, 1903.
6 S. Song and A. Singh, *Anal. Bioanal. Chem.*, 2006, **384**, 41.
7 H. Cui, K. Horiuchi, P. Dutta and C. F. Ivory, *Anal. Chem.*, 2005, **77**, 1303.
8 C. Li, Y. Yang, H. G. Craighead and K. H. Lee, *Electrophoresis*, 2005, **26**, 1800.
9 O. Hofmann, D. Che, K. A. Cruickshank and U. R. Müller, *Anal. Chem.*, 1998, **71**, 678.
10 J. Lichtenberg, E. Verpoorte and N. F. de Rooij, *Electrophoresis*, 2001, **22**, 258.
11 H. Yang and R.-L. Chien, *J. Chromatogr., A*, 2001, **924**, 155.
12 P. Gebauer and P. Bocek, *Electrophoresis*, 2002, **23**, 3858.
13 B. Jung, R. Bharadwaj and J. G. Santiago, *Anal. Chem.*, 2006, **78**, 2319.
14 J. G. Shackman and D. Ross, *Electrophoresis*, 2007, **28**, 556.
15 K. M. Balss, W. N. Vreeland, K. W. Phinney and D. Ross, *Anal. Chem.*, 2004, **76**, 7243.
16 S. J. Hoebel, K. M. Balss, B. J. Jones, C. D. Malliaris, M. S. Munson, W. N. Vreeland and D. Ross, *Anal. Chem.*, 2006, **78**, 7186.
17 S. M. Kim, G. J. Sommer, M. A. Burns and E. F. Hasselbrink, *Anal. Chem.*, 2006, **78**, 8028.
18 D. Ross and L. E. Locascio, *Anal. Chem.*, 2002, **74**, 2556.
19 P. H. Humble, R. T. Kelly, A. T. Woolley, H. D. Tolley and M. L. Lee, *Anal. Chem.*, 2004, **76**, 5641.
20 W. S. Koegler and C. F. Ivory, *J. Chromatogr., A*, 1996, **726**, 229.
21 S.-L. Lin, Y. Li, H. D. Tolley, P. H. Humble and M. L. Lee, *J. Chromatogr., A*, 2006, **1125**, 254.
22 S.-L. Lin, Y. Li, A. T. Woolley, M. L. Lee, H. D. Tolley and K. F. Warnick, *Electrophoresis*, 2008, **29**, 1058.
23 M. M. Meighan, S. J. R. Staton and M. A. Hayes, *Electrophoresis*, 2009, **30**, 852.
24 X. Sun, P. B. Farnsworth, H. D. Tolley, K. F. Warnick, A. T. Woolley and M. L. Lee, *J. Chromatogr., A*, 2009, **1216**, 159.
25 J. M. Burke, Z. Huang and C. F. Ivory, *Anal. Chem.*, 2009, **81**, 8236.
26 J. M. Burke, C. D. Smith and C. F. Ivory, *Electrophoresis*, 2010, **31**, 902.
27 Z. Huang and C. F. Ivory, *Anal. Chem.*, 1999, **71**, 1628.
28 Y.-C. Wang, A. L. Stevens and J. Han, *Anal. Chem.*, 2005, **77**, 4293.
29 K. Zhou, M. L. Kovarik and S. C. Jacobson, *J. Am. Chem. Soc.*, 2008, **130**, 8614.
30 A. Höltzel and U. Tallarek, *J. Sep. Sci.*, 2007, **30**, 1398.
31 S. J. Kim, L. D. Li and J. Han, *Langmuir*, 2009, **25**, 7759.
32 S. M. Kim, M. A. Burns and E. F. Hasselbrink, *Anal. Chem.*, 2006, **78**, 4779.
33 J. C. McDonald, D. C. Duffy, J. R. Anderson, D. T. Chiu, H. Wu, O. J. A. Schueller and G. M. Whitesides, *Electrophoresis*, 2000, **21**, 27.
34 A. Arora, J. C. T. Eijkel, W. E. Morf and A. Manz, *Anal. Chem.*, 2001, **73**, 3282.
35 F. Mavré, K.-F. Chow, E. Sheridan, B.-Y. Chang, J. A. Crooks and R. M. Crooks, *Anal. Chem.*, 2009, **81**, 6218.
36 O. Ordeig, N. Godino, J. del Campo, F. X. Munoz, F. Nikolajeff and L. Nyholm, *Anal. Chem.*, 2008, **80**, 3622.
37 W. Hellmich, J. Regtmeier, T. T. Duong, R. Ros, D. Anselmetti and A. Ros, *Langmuir*, 2005, **21**, 7551.
38 K.-D. Huang and R.-J. Yang, *Electrophoresis*, 2008, **29**, 4862.
39 S. J. Kim, Y.-A. Song and J. Han, *Chem. Soc. Rev.*, 2010, **39**, 912.
40 D. Maynes, J. Tenny, B. W. Webb and M. L. Lee, *Electrophoresis*, 2008, **29**, 549.